Cancer Immunol Immunother (2017) 66:1229–1241
DOI 10.1007/s00262-017-2016-9

ORIGINAL ARTICLE

Paracrine release of IL-2 and anti-CTLA-4 enhances the ability of artificial polymer antigen-presenting cells to expand antigen-specific T cells and inhibit tumor growth in a mouse model

Lei Zhang[1] · Limin Wang[1] · Khawar Ali Shahzad[1] · Tao Xu[1] · Xin Wan[1] · Weiya Pei[1] · Chuanlai Shen[1]

Received: 17 October 2016 / Accepted: 6 May 2017 / Published online: 13 May 2017

Abstract Accumulating evidence indicates that bead-based artificial antigen-presenting cells (aAPCs) are a powerful tool to induce antigen-specific T cell responses in vitro and in vivo. To date, most conventional aAPCs have been generated by coupling an antigen signal (signal 1) and one or two costimulatory signals, such as anti-CD28 with anti-LFA1 or anti-4-1BB (signal 2), onto the surfaces of cell-sized or nanoscale magnetic beads or polyester latex beads. The development of a biodegradable scaffold and the combined use of multiple costimulatory signals as well as third signals for putative clinical applications is the next step in the development of this technology. Here, a novel biodegradable aAPC platform for active immunotherapy was developed by co-encapsulating IL-2 and anti-CTLA-4 inside cell-sized polylactic-co-glycolic acid microparticles (PLGA-MPs) while co-coupling an H-2K^b/TRP2-Ig dimer and anti-CD28 onto the surface. Cytokines (activating signal) and antibodies (anti-inhibition signal) were efficiently co-encapsulated in PLGA-MP-based aAPCs and co-released without interfering with each other. The targeted, sustained co-release of IL-2 and anti-CTLA-4 achieved markedly enhanced, synergistic effects in activating and expanding tumor antigen-specific T cells both in vitro and in vivo, as well as in inhibiting tumor growth in a mouse melanoma model, as compared with conventional two-signal aAPCs and IL-2 or anti-CTLA-4 single-released aAPCs. These data revealed the feasibility and importance of the paracrine release of multiple costimulatory molecules and cytokines from biodegradable aAPCs and thus provide a proof of principle for the future use of polymeric aAPCs for active immunotherapy of tumors and infectious diseases.

Keywords Artificial antigen-presenting cells · PLGA-MPs · IL-2 · Anti-CTLA-4 · Active immunotherapy

Abbreviations

7-AAD	7-amino-actinomycin D
aAPCs	Artificial antigen-presenting cells
MNPs	Micro- and nanoparticles
MPs	Microparticles
PEI	Polyethylenimine
PLGA	Polylactic-co-glycolic acid
pMHC	Peptide-major histocompatibility complex
TRP2	Tyrosinase-related protein 2

Introduction

Efficiently activating and expanding antigen-specific T cells is a fundamental strategy of immunotherapy for persistent infections [1, 2] and cancers [3–5]. Although antigen-presenting cells (APCs), most notably dendritic cells, are powerful tools that facilitate active immune responses and have been used in the previous two decades, therapies with natural APCs in clinical settings have suffered from several issues, including their cumbersome generation and biosafety concerns [6, 7]. Therefore, as an alternative strategy, artificial APCs (aAPCs) have been proposed and rapidly developed to induce therapeutic cellular immunity

Electronic supplementary material The online version of this article (doi:10.1007/s00262-017-2016-9) contains supplementary material, which is available to authorized users.

✉ Chuanlai Shen
chuanlaishen@seu.edu.cn

[1] Department of Microbiology and Immunology, Medical School, Southeast University, 87 Dingjiaqiao Rd, Nanjing 210009, Jiangsu, People's Republic of China

[8–10]. aAPCs encompass both cell-based [11–13] and acellular technologies [10, 14–16]. Cell-free aAPCs were originally prepared by covalently coupling peptide–MHC complex (pMHC) and the CD28 ligand onto cell-sized or nanoscale magnetic beads or polyester latex beads [15–20]. To fully replace natural APCs, optimal aAPCs must present three signals: the first signal is from antigenic peptides that are loaded in MHC molecules to target antigen-specific T cells; the second signal is from a group of costimulatory molecules (membrane-bound proteins) that elicit T cell activation and proliferation; and the third signal is from cytokines that play crucial roles in T cell expansion, differentiation and survival. Recent studies on acellular aAPC fabrication have primarily focused on application of the first and second signals onto rigid beads, e.g., magnetic or latex beads. For putative clinical applications, future bead-based aAPC processes require the development of a biodegradable scaffold and the combined use of multiple costimulatory signals and third signals.

Polylactic-co-glycolic acid (PLGA) is a biodegradable, biocompatible and non-toxic polymer that has been approved by the United States Food and Drug Administration for therapeutic use in humans. PLGA micro- and nanoparticles (MNPs) have been successfully used to deliver peptides, proteins, and drugs via encapsulation and/or surface coupling [21, 22]. Herein, both IL-2 and anti-CTLA-4 were initially co-encapsulated into cell-sized PLGA-MPs to concurrently present an activating signal and anti-inhibitory signal on T cells by paracrine delivery, and an H-2K^b/TRP2-Ig dimer and anti-CD28 were co-coupled on the surface. The encapsulation and co-release efficiencies of IL-2 and anti-CTLA-4 were analyzed and followed by the evaluation of their synergistic effects in activating and expanding tumor antigen-specific T cells, both in vitro and in vivo, and in inhibiting tumor growth in a mouse melanoma model.

Materials and methods

Mice, cell lines and peptides

Female C57BL/6J mice at 8–10 weeks of age were obtained from the Comparative Medicine Center of Yangzhou University (Yangzhou, China) and maintained at the specific-pathogen-free Laboratory Animal Centre of Southeast University (Nanjing, China). Animal welfare and experimental procedures were performed in accordance with the Guide for the Care and Use of Laboratory Animals (Ministry of Science and Technology of China, 2006) and were approved by the Animal Ethics Committee of Southeast University. All cell lines were from the Cell Bank of Type Culture Collection of Chinese Academy of Sciences. The $TRP2_{180–188}$ (SVYDFFVWL) and $OVA_{257–264}$ (SIINFEKL) peptides were synthesized by GenScript Corp (Nanjing, China) with a purity of >95%.

Fabrication of PLGA-MPs encapsulated with IL-2 and anti-CTLA-4

PLGA-MPs were fabricated using a double-emulsion water-in-oil-in-water (W1/O/W2) method as previously described [23, 24], with modifications. Briefly, 100 mg of PLGA (Daigang Company, Jinan, China) was initially dissolved in 5 mL of dichloromethane (oil phase, O); this was followed by the addition of 200 μL of 0.1 M PBS (for blank MPs) or 200 μL of an aqueous solution containing 2.5 μg of IL-2 (PeproTech) and/or 12.5 mg of anti-CTLA-4 (BioXCell) as an internal water phase (W1). Then, the W1/O emulsion was formed by sonicating the mixture for 30 s at 20 kHz and 30% amplitude with a probe sonicator (Sonics & Materials). The primary W1/O emulsion was quickly mixed with 5 mL of a 4% (w/v) polyvinyl alcohol solution (PVA, Sigma) (external water phase, W2) and homogenized (T-18 digital ULTRA-TURRAX® IKA) for 30 min at 6000 rpm. Then, 5 mL of deionized water was added and the solution was stirred overnight at room temperature to evaporate the dichloromethane. The final solution was centrifuged at 3000 rpm for 5 min to collect microparticles (MPs). The harvested MPs were washed to remove PVA, activated using 1-ethyl-3-(3-dimethylaminopropyl) carbodiimide hydrochloride (EDC) and *N*-hydroxysuccinimide (NHS) (Sigma), and added dropwise to the polyethylenimine (PEI, Sigma) solution with magnetic stirring and incubated for another 2 h at 20 °C. Finally, PEI-conjugated MPs were washed twice with deionized water and stored at 4 °C for use. In parallel, control PLGA-MPs were also generated using similar methods, including MPs without encapsulation and MPs encapsulated with only IL-2 or anti-CTLA-4.

Characterization of PLGA-MPs

The morphology of the resulting PLGA-MPs was characterized by using scanning electron microscopy (SEM, ZEISS EVO 18). The size distribution was determined by analyzing micrographs using NIH ImageJ (NIH), and the zeta potential was measured using a PALS Zeta instrument (Brookhaven Instruments Corporation).

Encapsulation and sustained release of IL-2 and anti-CTLA-4

To determine the amount of IL-2 and anti-CTLA-4 encapsulated into PLGA-MPs, 1×10^7 PLGA-MPs were re-suspended in 1 mL of a 0.1 M NaOH/0.5% SDS solution. After a 24-h incubation at 37 °C on a shaker, the suspension was

centrifuged for 5 min at 3000 rpm. The supernatant was collected and subjected to quantitative detection of IL-2 and anti-CTLA-4 with ELISA kits (eBiosciences) according to the manufacturer's protocols.

To monitor the dynamic release of IL-2 and anti-CTLA-4 from the PLGA-MPs, 1×10^7 PLGA-MPs were re-suspended in 1 mL of sterile 0.1 M PBS buffer and incubated on a rotator (200 rpm) at 37 °C. At the indicated time points, the supernatant was collected after centrifugation, and an equal volume of fresh medium was used to re-suspend the MPs. The amount of IL-2 and anti-CTLA-4 in the supernatant was quantified using ELISA kits as described.

Characterization of the capacity of PLGA-MPs to couple proteins and mAbs

PLGA-MPs (1×10^8) were incubated with a series of 1 mL solutions of PBS containing the indicated amounts of BSA for 24 h at 4 °C with rotation. After centrifugation at 3000 rpm for 5 min, the supernatant was collected for the detection of protein that was unbound to MPs by using a micro-BCA protein assay kit (Thermo Fisher). The amount of protein coupled to the MPs was then calculated. In addition, 10 μg of FITC-anti-hamster IgG (eBiosciences) was incubated with 1×10^8 blank PLGA-MPs, BSA-blocked MPs, or PEI-free MPs overnight with rotation at 4 °C. After being washed with deionized water, the MPs were measured via fluorescence microscopy and flow cytometry.

Preparation and phenotypic analysis of aAPCs

H-2K^b/TRP2-Ig dimers were prepared by mixture of H-2K^b-Ig Dimer X (BD) with the TRP2$_{180–188}$ peptide for 48 h at 4 °C according to the manufacturer's instructions. PLGA-MPs encapsulated with IL-2 and anti-CTLA-4 as well as those surface-modified with PEI were fabricated as described. Then, the MPs (1×10^8) were incubated with peptide-loaded H-2K^b-Ig (H-2K^b/TRP2-Ig dimers) (10 μg) and anti-CD28 mAbs (10 μg) (eBiosciences) in sterile 0.1 M PBS for 24 h at 4 °C on a rotator. The resulting MPs were incubated in blocking buffer (0.1 M PBS containing 10% BSA) at 4 °C for another 24 h with rotation. Finally, the suspension was centrifuged, and the particles were harvested. After being washed with PBS three times, the resultant aAPCs, termed aAPC$^{IL\text{-}2+anti\text{-}CTLA4}$, were re-suspended in sterile PBS, stored at 4 °C and used within 24 h. In parallel, several control aAPCs were also generated in a similar manner, including aAPC, aAPC$^{IL\text{-}2}$ and aAPC$^{anti\text{-}CTLA\text{-}4}$.

To analyze the phenotypes, 1×10^7 aAPCs were stained with 1 μg of PE-anti-mouse H-2K^b (eBiosciences) and 1 μg of FITC-anti-hamster IgG (binds to anti-CD28) for 30 min at 4 °C. After another washing step, for each sample, 2×10^5 particles were analyzed with a FACSCalibur flow cytometer (BD), and data were analyzed with FlowJo software (Tree Star, Inc.).

In vitro expansion of TRP2$_{180–188}$-specific CD8$^+$ T cells by aAPCs

Splenocytes were harvested from naïve C57BL/6J mice, and mononuclear cells were enriched by density gradient centrifugation. The splenocytes (10^5 cells/well) were co-cultured with blank PLGA-MPs (blocked with BSA), aAPC, aAPC$^{IL\text{-}2}$, aAPC$^{anti\text{-}CTLA4}$, aAPC$^{IL\text{-}2+anti\text{-}CTLA4}$, aAPC plus exogenous IL-2/anti-CTLA4, or aAPC$^{IL\text{-}2}$ plus aAPC$^{anti\text{-}CTLA4}$ in a 96-well round-bottom plate at a density of 10^5 beads for each type of aAPC per well. Co-cultures were maintained in RPMI 1640 medium supplemented with 10% FBS in the absence of IL-2 (50 U/mL IL-2 was supplied in the blank PLGA-MPs group; 0.162 ng IL-2/0.92 μg anti-CTLA-4 was supplied in the aAPC plus exogenous IL-2/anti-CTLA4 group) and incubated in a humidified incubator with 5% CO_2 at 37 °C for 1 week. Then, the co-cultures were harvested to analyze the frequency of TRP2$_{180–188}$-specific CD8$^+$ T cells by flow cytometry. Briefly, cells were first blocked with anti-mouse CD16/CD32 (BD) for 30 min and then incubated with a mixture of H-2K^b/TRP2-Ig dimers and allophycocyanin (APC)-anti-mouse IgG1 (BD) for 1 h at 4 °C in the dark. After washing, FITC-anti-mouse CD8 and PE-anti-mouse CD3 (eBiosciences) were added for another 30-min incubation. Finally, cells were analyzed by flow cytometry after washing.

Cytotoxicity assay

After a 1-week incubation with aAPCs, splenocytes were harvested for use as effector cells. The mouse melanoma cell line B16 (H-2K^{b+}/TRP2$^+$), fibrosarcoma cell line S180 (H-2K^{b+}/TRP2$^-$), and myeloma cell line SP2/0 (H-2K^{b-}/TRP2$^-$) were used as target cells (1×10^4 cells/well). The cytotoxicity assay was then performed as previously described [20].

In vivo expansion of TRP2$_{180–188}$-specific CD8$^+$ T cells and tumor inhibition by an aAPC infusion

On day 0, C57BL/6J mice were s.c. injected in the right flank with B16 cells (or S180 cells) at a dose of 1×10^6 cells per mouse. Mice were then randomly assigned to 1 of 5 groups and infused via the tail vein with blank PLGA-MPs, aAPC, aAPC$^{IL\text{-}2}$, aAPC$^{anti\text{-}CTLA4}$, aAPC$^{IL\text{-}2+anti\text{-}CTLA4}$, aAPC plus systemic use of IL-2/anti-CTLA4 (16.2 ng/92 μg), or aAPC$^{IL\text{-}2}$ plus aAPC$^{anti\text{-}CTLA4}$ on days 7, 9 and 11 at a dose of 1×10^7 MPs for each type of aAPC (0.9 mg PLGA) per mouse per time point. On day 7 (before treatment) and day

28 (after treatment), peripheral blood was collected from orbital vein. The spleen and tumors were also isolated from each mouse on day 28. Blood, spleens and tumors were then processed to single-cell suspensions, and this was followed by $TRP2_{180–188}$-specific $CD8^+$ T cell detection. The single-cell suspensions derived from tumor tissues were prepared as previously described [25], except that tumor tissues minced into small pieces were digested with collagenase type VIII (1.5 mg/mL, Sigma) for 2 h at 37 °C with gentle agitation.

Tumor growth was monitored at 3-day intervals using a digital caliper. The tumor volume was calculated by the modified ellipsoidal formula: $V = (\text{length} \times \text{width}^2)/2$ [26]. Mice were monitored daily for survival and were killed when the tumor length exceeded 20 mm.

In vivo tracking and tissue distribution of $aAPC^{IL\text{-}2+anti\text{-}CTLA4}$

Indocyanine green-encapsulated $aAPC^{IL\text{-}2+anti\text{-}CTLA4}$ was generated as described in our previous work [27] and injected i.v. into C57BL/6J mice (1×10^7/mouse) on day 7 after B16 cell challenge. The mice were then anesthetized by isoflurane inhalation and imaged using the Maestro in vivo fluorescence imaging system (Cri, Inc., Woburn, MA, USA) at various time points. Images were captured at an excitation wavelength of 635 nm and an emission wavelength of 665–695 nm with an exposure time of 40 s. At the 2-h time point after injection, the heart, liver, kidneys, lungs, spleen, and lymph nodes were surgically dissected for ex vivo imaging.

Statistical analyses

Statistical analyses were performed using GraphPad Prism 6.0 (La Jolla). All data are presented as the mean ± SD. The frequencies of antigen-specific T cells were compared between groups by using a two-tailed, unpaired Student's *t* test. The release profiles of IL-2 and anti-CTLA-4, as well as the tumor growth curves, were analyzed by Wilcoxon signed rank tests and two-tailed, paired Student's *t* tests. To determine the survival curve of mice, a Kaplan–Meier graph was constructed, and a log-rank comparison of the groups was used to calculate the *P* values. $P < 0.05$ was considered significant.

Results

Characterization of PLGA-MPs

The PLGA-MPs fabricated herein displayed a spherical shape and smooth surface topography, with a uniform size of 4.5 ± 1.2 μm, as revealed by SEM (Fig. 1a, b). Conjugation of PEI onto the surface of MPs led to a mean zeta potential of 36.2 ± 5.6 mV, as detected by the PALS zeta instrument, thus suggesting a strong capacity of MPs to covalently couple proteins (Fig. 1c).

Encapsulation efficiency and release profile of IL-2 and anti-CTLA-4 in PLGA-MPs

Approximately 20 ng of IL-2 and 100 μg of anti-CTLA-4 were encapsulated into 1×10^7 beads of $PLGA\text{-}MP^{IL\text{-}2}$ and $PLGA\text{-}MP^{anti\text{-}CTLA4}$, respectively, under the current process conditions. The encapsulation efficiency was approximately 80% for both IL-2 and anti-CTLA-4. Moreover, $PLGA\text{-}MP^{IL\text{-}2+anti\text{-}CTLA4}$ displayed encapsulation efficiencies of IL-2 and anti-CTLA-4 similar to that of $PLGA\text{-}MP^{IL\text{-}2}$ or $PLGA\text{-}MP^{anti\text{-}CTLA4}$. No significant interference was found between the cytokine and mAb when they were concurrently encapsulated inside PLGA-MPs.

Over 28 days, both IL-2 and anti-CTLA-4 were released from $PLGA\text{-}MP^{IL\text{-}2+anti\text{-}CTLA4}$ in a sustained manner. The dynamic release curve of IL-2 from $PLGA\text{-}MP^{IL\text{-}2+anti\text{-}CTLA4}$ was similar to that from $PLGA\text{-}MP^{IL\text{-}2}$, without significant differences, as analyzed by Wilcoxon signed rank tests and two-tailed, paired Student's t tests (Fig. 1d). The same phenomenon was also observed in the release assay of anti-CTLA-4 (Fig. 1e). The total cumulative IL-2 released from 1×10^7 beads of $PLGA\text{-}MP^{IL\text{-}2}$ or $PLGA\text{-}MP^{IL\text{-}2+anti\text{-}CTLA4}$ was nearly 16.2 ng, whereas the cumulative anti-CTLA-4 released from $PLGA\text{-}MP^{anti\text{-}CTLA4}$ or $PLGA\text{-}MP^{IL\text{-}2+anti\text{-}CTLA4}$ was approximately 92 μg over 28 days. The cumulative release efficiency was approximately 81% for IL-2 and 92% for anti-CTLA-4.

Capacity of PLGA-MPs to couple protein

As shown in Fig. 2a, the maximum amount of BSA loaded onto 5×10^6 beads of PEI-conjugated (surface-modified) PLGA-MPs was nearly 71 μg. Furthermore, FITC-anti-hamster IgG was also successfully immobilized onto the surface-modified PLGA-MPs, but not onto PEI-free (un-modified) PLGA-MPs (Fig. 2b). As analyzed by flow cytometry, surface-modified PLGA-MPs displayed a marked fluorescence shift of FITC compared with the MPs that were blocked with BSA before FITC-anti-hamster IgG coating (Fig. 2c). These data demonstrated the strong capacity of surface-modified PLGA-MPs to couple protein and antibodies.

To determine the appropriate amount of anti-CD28 and $H\text{-}2K^b$-Ig for use in preparing aAPCs, PLGA-MPs (1×10^8) were incubated with the indicated amounts of anti-CD28 or $H\text{-}2K^b$-Ig overnight, blocked with BSA, and stained with FITC-anti-hamster IgG or PE-anti-$H\text{-}2K^b$ mAb. The results showed that the PLGA-MPs were able

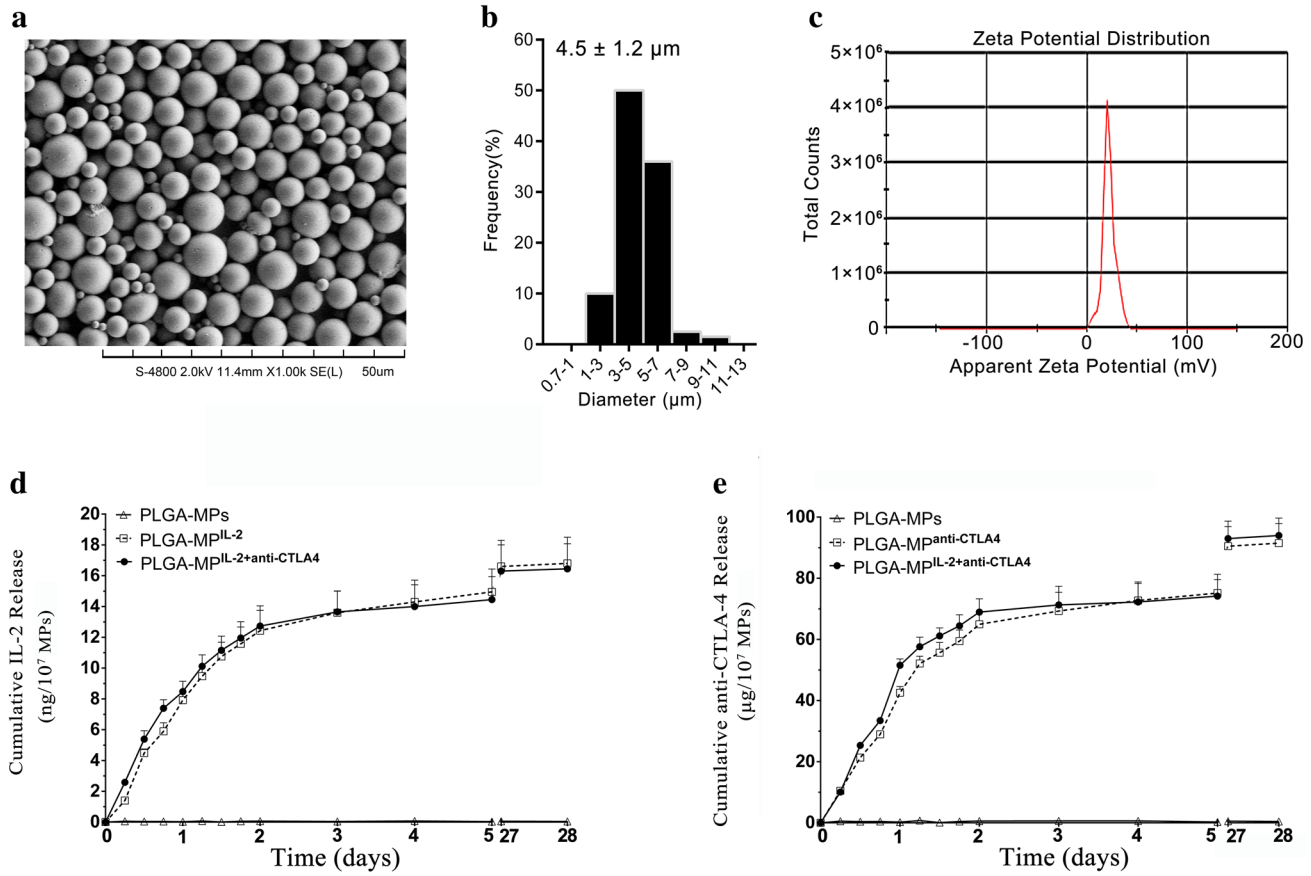

Fig. 1 Characterization of PLGA-MPs and release profiles of IL-2 and anti-CTLA-4 from PLGA-MPs. **a** Representative SEM image, **b** size distribution, and **c** zeta potential distribution of PLGA-MPs generated on-site. **d** Release profiles of IL-2 from blank PLGA-MPs, PLGA-MPs$^{IL\text{-}2}$, and PLGA-MPs$^{IL\text{-}2+anti\text{-}CTLA4}$ over 28 days. **e** Release profiles of anti-CTLA-4 from blank PLGA-MPs, PLGA-MPs$^{anti\text{-}CTLA4}$, and PLGA-MPs$^{IL\text{-}2+anti\text{-}CTLA4}$ over 28 days

to couple anti-CD28 or H-2K^b-Ig and displayed a significant fluorescence shift of FITC at 5–20 μg of anti-CD28 (Fig. 2d) or PE at 5–20 μg of H-2K^b-Ig (Fig. 2e). Finally, 10 μg of H-2K^b-Ig and 10 μg of anti-CD28 were used for the preparation of 1×10^8 aAPCs.

Phenotypic analyses and release profiles of IL-2 and anti-CTLA-4 for aAPCs

Four types of aAPCs were generated by co-coating H-2K^b/TRP2-Ig dimers and anti-CD28 mAbs onto PLGA-MP, PLGA-MP$^{IL\text{-}2}$, PLGA-MP$^{anti\text{-}CTLA4}$, or PLGA-MP$^{IL\text{-}2+anti\text{-}CTLA4}$. The mean sizes of these aAPCs were not markedly different from those of blank PLAG-MPs, but their zeta potential returned to the zero position (Fig. 3a, Supplementary Fig. 1). As shown in Fig. 3b, a comparable fluorescent shift for H-2K^b/TRP2-Ig or anti-CD28 was found across the groups. The release profile of IL-2 from aAPC$^{IL\text{-}2+anti\text{-}CTLA4}$ was similar to that from aAPC$^{IL\text{-}2}$ (Fig. 3c). A similar phenomenon was also observed for the anti-CTLA-4 release profiles (Fig. 3d).

Co-release of IL-2 and anti-CTLA-4 from aAPCs enhanced the expansion and cytotoxicity of melanoma antigen-specific CD8$^+$ T cells in vitro

After a 1-week co-culture of naïve splenocytes with blank PLGA-MPs, aAPC, aAPC$^{IL\text{-}2}$, aAPC$^{anti\text{-}CTLA4}$, and aAPC$^{IL\text{-}2+anti\text{-}CTLA4}$, the frequency of TRP2$_{180–188}$-specific CD8$^+$ T cells in the CD8$^+$ T cell populations were detected by H-2K^b/TRP2-Ig dimer staining and are summarized in Fig. 4a (top row). As compared with the blank PLGA-MPs group, TRP2$_{180–188}$-specific CD8$^+$ T cells were expanded approximately 26 times by aAPC, 69 times by aAPC$^{IL\text{-}2}$, 77 times by aAPC$^{anti\text{-}CTLA4}$, and 128 times by aAPC$^{IL\text{-}2+anti\text{-}CTLA4}$ over 7 days under the current co-culture conditions without exogenous IL-2. The ability of aAPC$^{IL\text{-}2+anti\text{-}CTLA4}$ to expand antigen-specific T cells was enhanced nearly fivefold relative to that of conventional two-signal aAPCs. As a non-cognate antigen staining control, the OVA$_{257–264}$ antigen-specific CD8$^+$ T cells (OVA-dimer$^+$ CTLs) increased only slightly in the four aAPC groups compared with the PLGA-MPs group (Fig. 4a, bottom row).

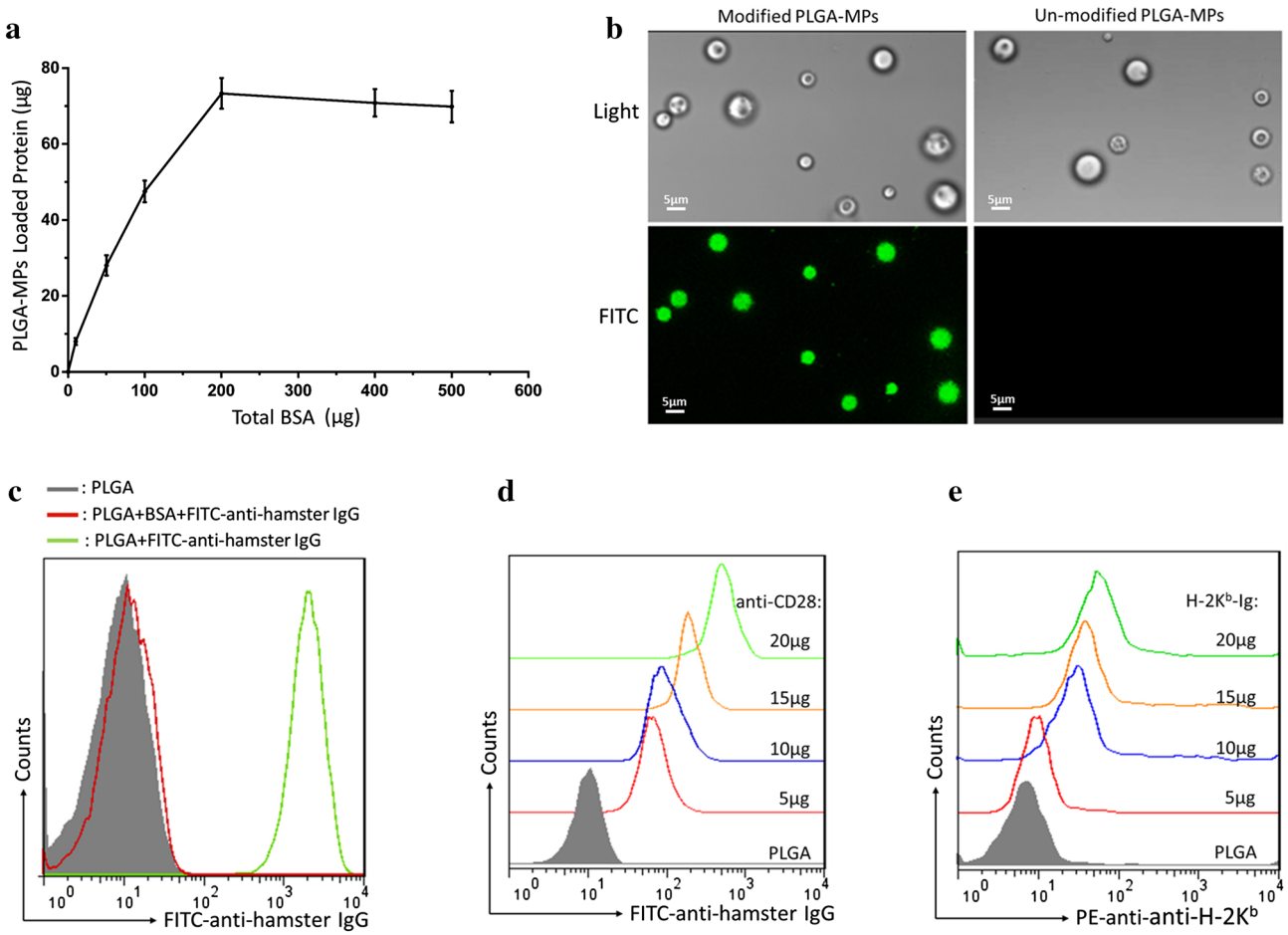

Fig. 2 Capacity of PLGA-MPs to couple proteins. **a** The amount of BSA coupled onto the surface of PLGA-MPs (5×10^6) was detected via micro-BCA protein assays. **b** FITC-anti-hamster IgG was coupled onto the surface of PLGA-MPs and detected with a fluorescence microscope. *Green* fluorescence was observed on the surface-modified PLGA-MPs, but not on the un-modified PLGA-MPs. **c** Surface-modified PLGA-MPs were incubated with FITC-anti-hamster IgG before (*green*) and after (*red*) blocking with 30% BSA and then detected by flow cytometry. Furthermore, PLGA-MPs (1×10^8) were incubated with the indicated amounts of anti-CD28 or H-2K^b-Ig overnight, blocked with BSA, and then stained with FITC-anti-hamster IgG (binds to anti-CD28) or PE-anti-H-2K^b. The fluorescence shift of FITC (**d**) or PE (**e**) was detected in a range from 5 to 20 μg of anti-CD28 or H-2K^b-Ig

As shown in Fig. 4c, aAPC$^{IL\text{-}2+anti\text{-}CTLA4}$ elicited a much greater cytotoxicity of splenocytes against B16 cells than aAPC$^{IL\text{-}2}$, aAPC$^{anti\text{-}CTLA4}$, or aAPC at various E:T ratios. In the nonspecific cytolysis controls, splenocytes from all groups showed less than 6% of baseline cytolysis against S180 cells and SP2/0 cells. The flow cytometric histograms of 7-AAD staining for B16 cells (Fig. 4e) and SP2/0 cells and S180 cells (Supplementary Fig. 2) in each cytolysis assay are presented.

In another independent experiment, naïve splenocytes were co-cultured for 7 days with the two-signal aAPCs exogenous IL-2/anti-CTLA-4, the mixture of aAPC$^{IL\text{-}2}$ and aAPC$^{anti\text{-}CTLA4}$, or aAPC$^{IL\text{-}2+anti\text{-}CTLA4}$. No significant differences were found across the three groups in the expansion and cytotoxicity of TRP2$_{180–188}$-specific CD8$^+$ T cells (Fig. 4b, d, f). Paracrine release of IL-2/anti-CTLA-4 appeared to have effects similar to the exogenous supply of IL-2/anti-CTLA-4 in co-cultures.

Paracrine co-release of IL-2 and anti-CTLA-4 from aAPCs augmented melanoma antigen-specific CTL responses and inhibited tumor growth in vivo

To further investigate the in vivo effects of aAPCs$^{IL\text{-}2+anti\text{-}CTLA4}$ inhibition of tumor growth, C57BL/6J mice were s.c. injected with B16 or S180 cells on day 0 and i.v. infused with blank PLGA-MPs, aAPC, aAPC$^{IL\text{-}2}$, aAPC$^{anti\text{-}CTLA4}$ or aAPC$^{IL\text{-}2+anti\text{-}CTLA4}$ on days 7, 9 and 11 as a preventive therapy (Fig. 5a). On day 7, the average sizes of the melanoma and fibrosarcoma were 1.998 ± 0.240 mm^3 and 1.041 ± 0.167 mm^3, respectively, before treatment. Furthermore, statistically

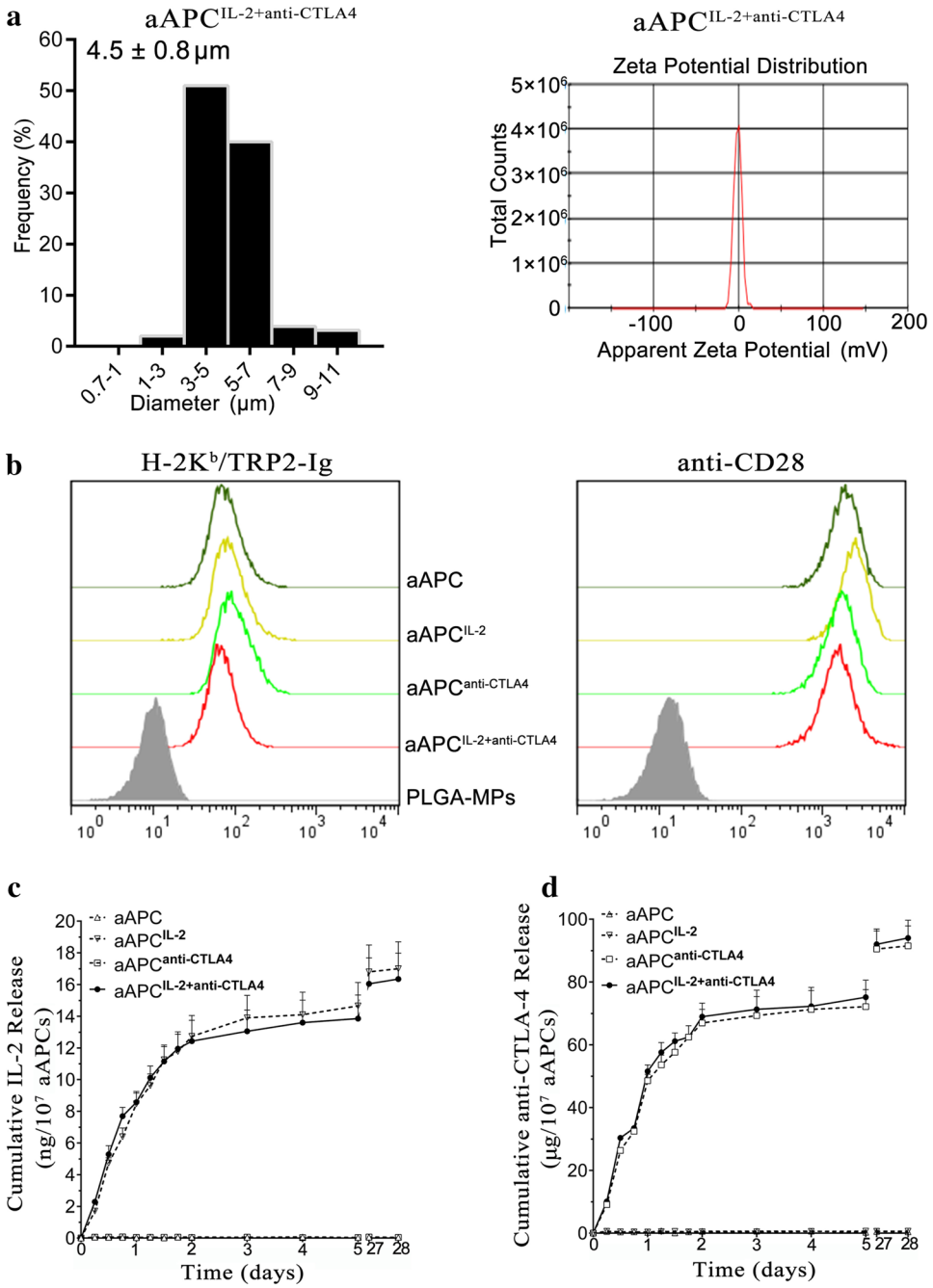

Fig. 3 Characterization of aAPCs. **a** Size distribution and zeta potential distribution of aAPC$^{IL\text{-}2+anti\text{-}CTLA4}$. **b** Phenotype analyses of aAPC, aAPC$^{IL\text{-}2}$, aAPC$^{anti\text{-}CTLA4}$, and aAPC$^{IL\text{-}2+anti\text{-}CTLA4}$. All types of aAPCs were stained with PE-anti-H-2K^b and FITC-anti-hamster IgG to detect the co-immobilization of H-2K^b/TRP2-Ig dimers and anti-CD28 mAbs onto PLGA-MPs. Blank PLGA-MPs that were pre-blocked with 30% BSA displayed baseline staining. **c**, **d** Release profiles of IL-2 and anti-CTLA-4 from the four types of aAPCs over the course of 28 days, as detected by ELISA kits

slower growth of the subcutaneous melanoma was found in the aAPC$^{IL\text{-}2+anti\text{-}CTLA4}$ group compared with the aAPC$^{anti\text{-}CTLA4}$ group ($P = 0.0120$), aAPC$^{IL\text{-}2}$ group ($P = 0.0095$), aAPC group ($P = 0.0079$) or blank PLGA-MPs group ($P = 0.0015$), as analyzed by Wilcoxon signed rank tests. On day 28, mice treated with aAPC$^{IL\text{-}2+anti\text{-}CTLA4}$ achieved the smallest tumor burden, with a mean size of 510 mm^3, whereas mice treated with aAPC$^{anti\text{-}CTLA4}$, aAPC$^{IL\text{-}2}$, aAPC, or blank PLGA-MPs had an average tumor size of 743, 850, 1185, and 1600 mm^3, respectively (Fig. 5b). The excised melanoma tissues from each group are presented in Supplementary Fig. 3. In parallel, fibrosarcoma growth was not obviously inhibited by the administration of aAPC$^{IL\text{-}2+anti\text{-}CTLA4}$ or other control aAPCs (Fig. 5c). Moreover, concurrent release of IL-2 and anti-CTLA-4 from aAPCs markedly delayed melanoma progression. The median survival times (MSTs) were 46, 41, 35, 31 and 22 days in the aAPC$^{IL\text{-}2+anti\text{-}CTLA4}$ group, aAPC$^{anti\text{-}CTLA4}$ group, aAPC$^{IL\text{-}2}$ group, aAPC group and blank PLGA-MPs group, respectively (Fig. 5d). In addition, aAPC$^{IL\text{-}2+anti\text{-}CTLA4}$ treatment also resulted in

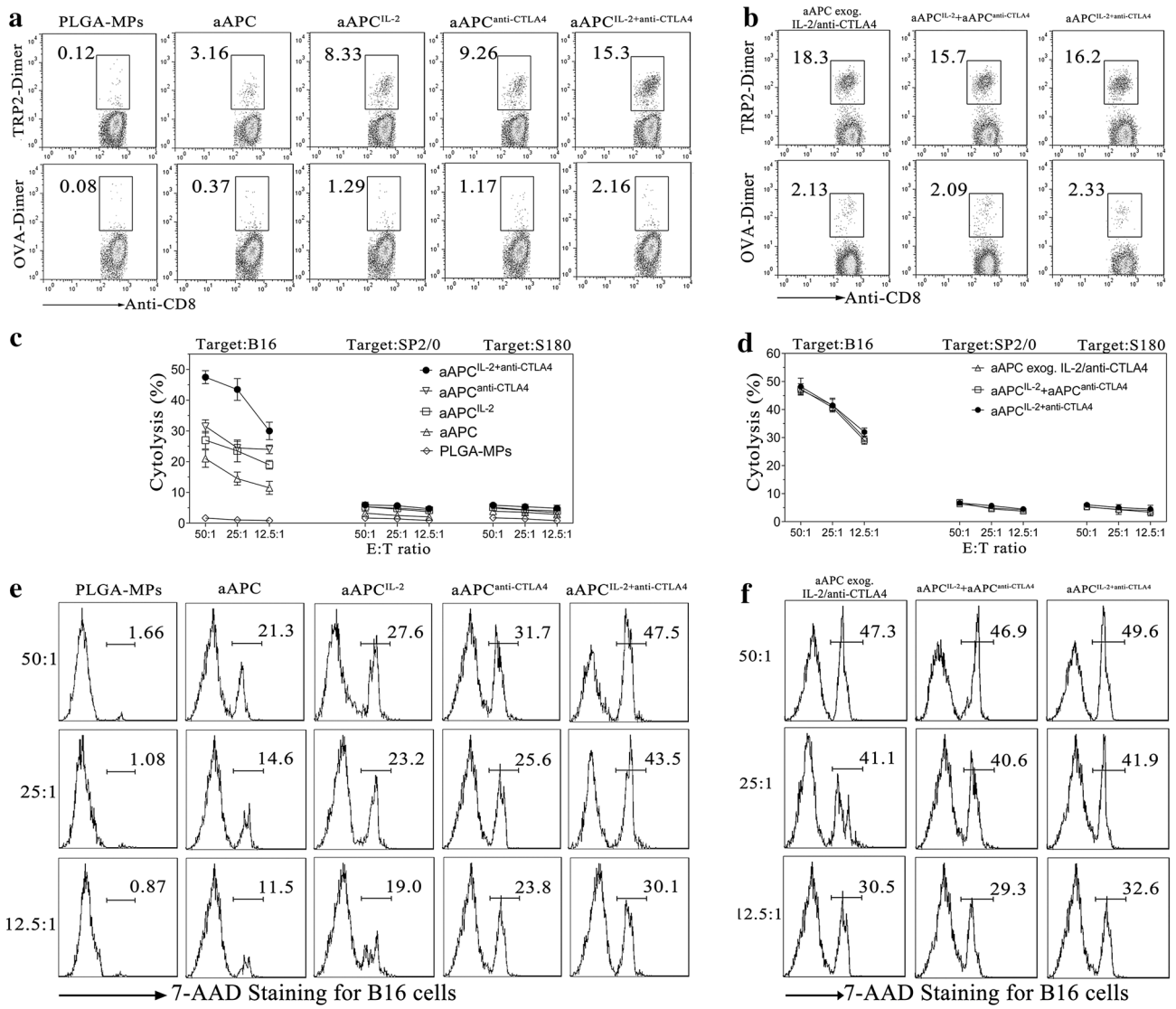

Fig. 4 Co-release of IL-2 and anti-CTLA-4 from aAPCs enhanced the expansion and cytotoxicity of melanoma antigen-specific $CD8^+$ T cells ex vivo. Naïve splenocytes from C57BL/6J mice were co-incubated for 7 days with blank PLGA-MPs and each type of aAPC. **a**, **b** The frequencies of $TRP2_{180–188}$-specific $CD8^+$ T cells (*top row*) and $OVA_{257–264}$-specific $CD8^+$ T cells (*bottom row*) in the co-culture group of blank PLGA-MPs, aAPC, $aAPC^{IL-2}$, $aAPC^{anti-CTLA4}$, $aAPC^{IL-2+anti-CTLA4}$, aAPC exogenous IL-2/anti-CTLA-4, or $aAPC^{IL-2}$ + $aAPC^{anti-CTLA4}$, as detected by H-$2K^b$/$TRP2_{180–188}$ dimer or H-$2K^b$/$OVA_{257–264}$ dimer staining. *Numbers in the top left of the flow cytometric dot plots* represent the percentage of $TRP2_{180–188}$ dimer- or $OVA_{257–264}$ dimer-positive cells in the $CD8^+$ T cell population. **c**, **d** Cytotoxicity of the splenocytes from the five co-culture groups of **a** and the three co-culture groups of **b**. The resulting splenocytes were further co-cultured with target cells for 4 h at various E:T ratios followed by 7-AAD staining to analyze the antigen-specific cytolysis of B16, SP2/0, and S180 tumor cells. **e**, **f** Representative flow cytometric histograms of 7-AAD staining for B16 cells for the five co-culture groups of **c** and the three co-culture groups of **d**. These data were from one representative experiment of three independent experiments

statistically slower growth of subcutaneous melanoma, as compared with combined injections of $aAPC^{IL-2}$ and $aAPC^{anti-CTLA4}$ ($P = 0.0260$) and injection of aAPCs plus systemic use IL-2/anti-CTLA-4 ($P = 0.0090$), as analyzed by Wilcoxon signed rank tests (Fig. 5e).

At the endpoint (day 28), the percentage of $TRP2_{180–188}$-specific $CD8^+$ T cells in peripheral blood was increased 51-fold (6.67 ± 0.26%) in the $aAPC^{IL-2+anti-CTLA4}$ group, 22-fold (2.83 ± 0.27%) in the $aAPC^{anti-CTLA4}$ group, 21-fold (2.67 ± 0.20%) in the $aAPC^{IL-2}$ group, and 15-fold (1.96 ± 0.09%) in the aAPC group, as compared with the percentage before treatment (0.13 ± 0.05%, data not shown) (Fig. 6a). In splenocyte suspensions, the frequencies in the $aAPC^{IL-2+anti-CTLA4}$, $aAPC^{anti-CTLA4}$, $aAPC^{IL-2}$, and aAPC

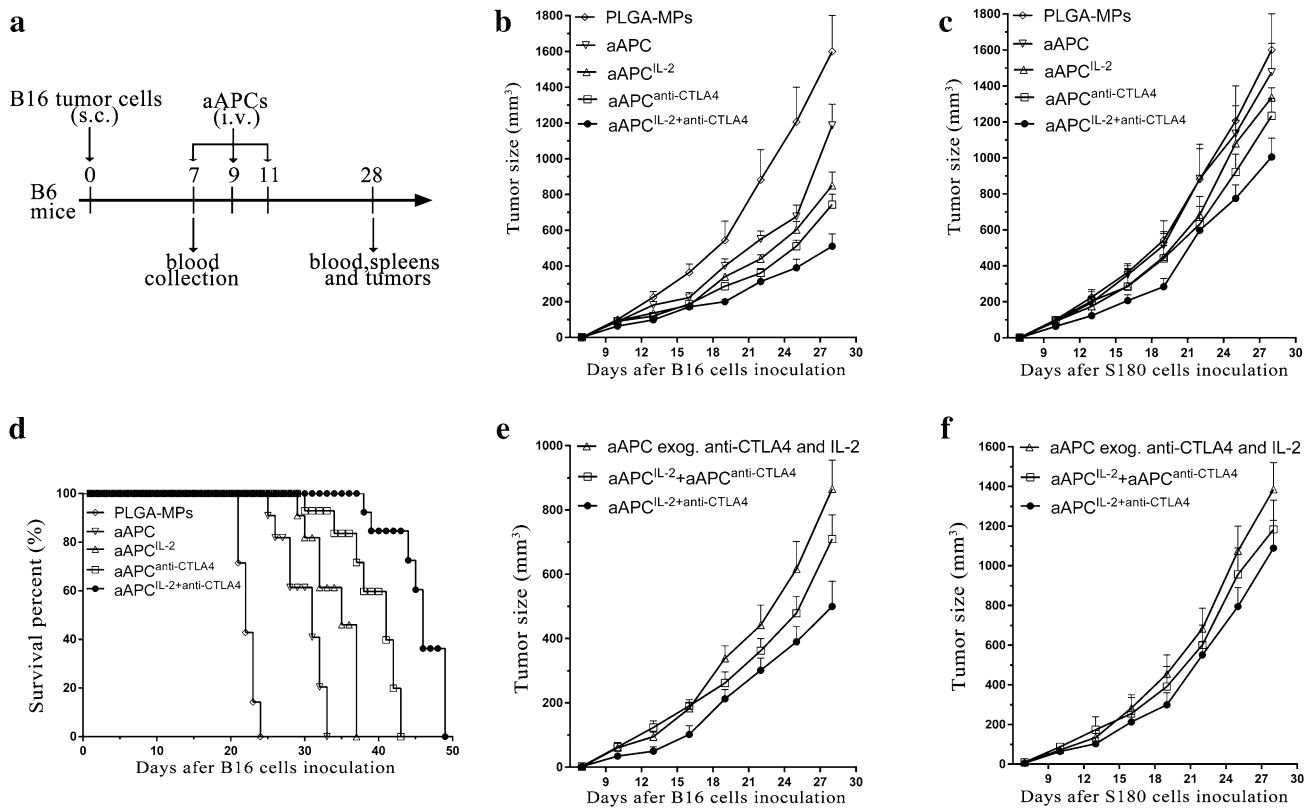

Fig. 5 Paracrine co-release of IL-2 and anti-CTLA-4 from aAPCs improved tumor inhibition in a mouse melanoma model. **a** Timeline for in vivo experiments. **b** Subcutaneous melanoma growth and **c** fibrosarcoma growth in the treatment group of blank PLGA-MPs, aAPC, $aAPC^{IL\text{-}2}$, $aAPC^{anti\text{-}CTLA4}$, or $aAPC^{IL\text{-}2+anti\text{-}CTLA4}$; $n = 7$ mice in each group. **d** Kaplan–Meier survival curves illustrate statistically improved survival rates in the $aAPC^{IL\text{-}2+anti\text{-}CTLA4}$ group relative to the $aAPC^{anti\text{-}CTLA4}$ group ($P = 0.0007$), $aAPC^{IL\text{-}2}$ group ($P < 0.0001$), aAPC group ($P < 0.0001$) and blank PLGA-MP group ($P < 0.0001$), as determined by a log-rank comparison. Mouse death was defined as tumor diameter exceeding 20 mm as well as natural death. The presented data were from one representative experiment of two independent experiments; $n = 7$ mice in each group in each experiment. **e** Subcutaneous melanoma growth and **f** fibrosarcoma growth in the treatment group of aAPC plus exogenous IL-2/anti-CTLA-4, $aAPC^{IL\text{-}2}$ + $aAPC^{anti\text{-}CTLA4}$, or $aAPC^{IL\text{-}2+anti\text{-}CTLA4}$. $n = 7$ mice in each group

groups were enhanced nearly 55-fold (6.03 ± 0.40%), 24-fold (2.65 ± 0.27%), 22-fold (2.43 ± 0.18%), and 16-fold (1.81 ± 0.16%), respectively, as compared with the blank PLGA-MPs group (0.11 ± 0.02%) (Fig. 6b). In single-cell suspensions derived from tumor tissues, the percentages were also much higher in the $aAPC^{IL\text{-}2+anti\text{-}CTLA4}$ group than the control groups (Fig. 6c). In addition, $aAPC^{IL\text{-}2+anti\text{-}CTLA4}$ treatment also resulted in significantly higher frequencies of $TRP2_{180–188}$-specific $CD8^+$ T cells than observed after combined injections of $aAPC^{IL\text{-}2}$/$aAPC^{anti\text{-}CTLA4}$ and injections of aAPCs plus systemic use of IL-2/anti-CTLA-4 in blood cells (Fig. 6d), spleen cells (Fig. 6e), and tumor-infiltrating cells (Fig. 6f). A significantly greater frequency of IFN-γ-secreting $CD8^+$ T cells in the tumor-infiltrating $CD8^+$ T cells, a clearly lower expression level of PD-1 onto tumor-infiltrating $CD8^+$ T cells, and a statistically lower percentage of regulatory T cells in tumor-infiltrating $CD4^+$ T cells were also observed in the $aAPC^{IL\text{-}2+anti\text{-}CTLA4}$ treatment group compared with the aAPCs exogenous IL-2/anti-CTLA4 group and combination group of $aAPC^{IL\text{-}2}$ and $aAPC^{anti\text{-}CTLA4}$ (Supplementary Fig. 4).

In vivo tracking and tissue distribution of $aAPC^{IL\text{-}2+anti\text{-}CTLA4}$

Whole-body fluorescence imaging showed that fluorescent $aAPC^{IL\text{-}2+anti\text{-}CTLA4}$ rapidly and selectively accumulated in the liver, spleen, kidney, lung, lymph nodes, and heart after i.v. injection into C57BL/6J mice challenged with B16 cells. A high fluorescence intensity was observed during the first 2 h and then gradually declined with a retention time of up to 24 h in mice (Supplementary Fig. 5a). As displayed by ex vivo imaging of excised organs at the 2-h time point after injection, aAPCs mainly accumulated in the liver, spleen and kidney; a weak fluorescence signal was observed in the lungs (Supplementary Fig. 5b).

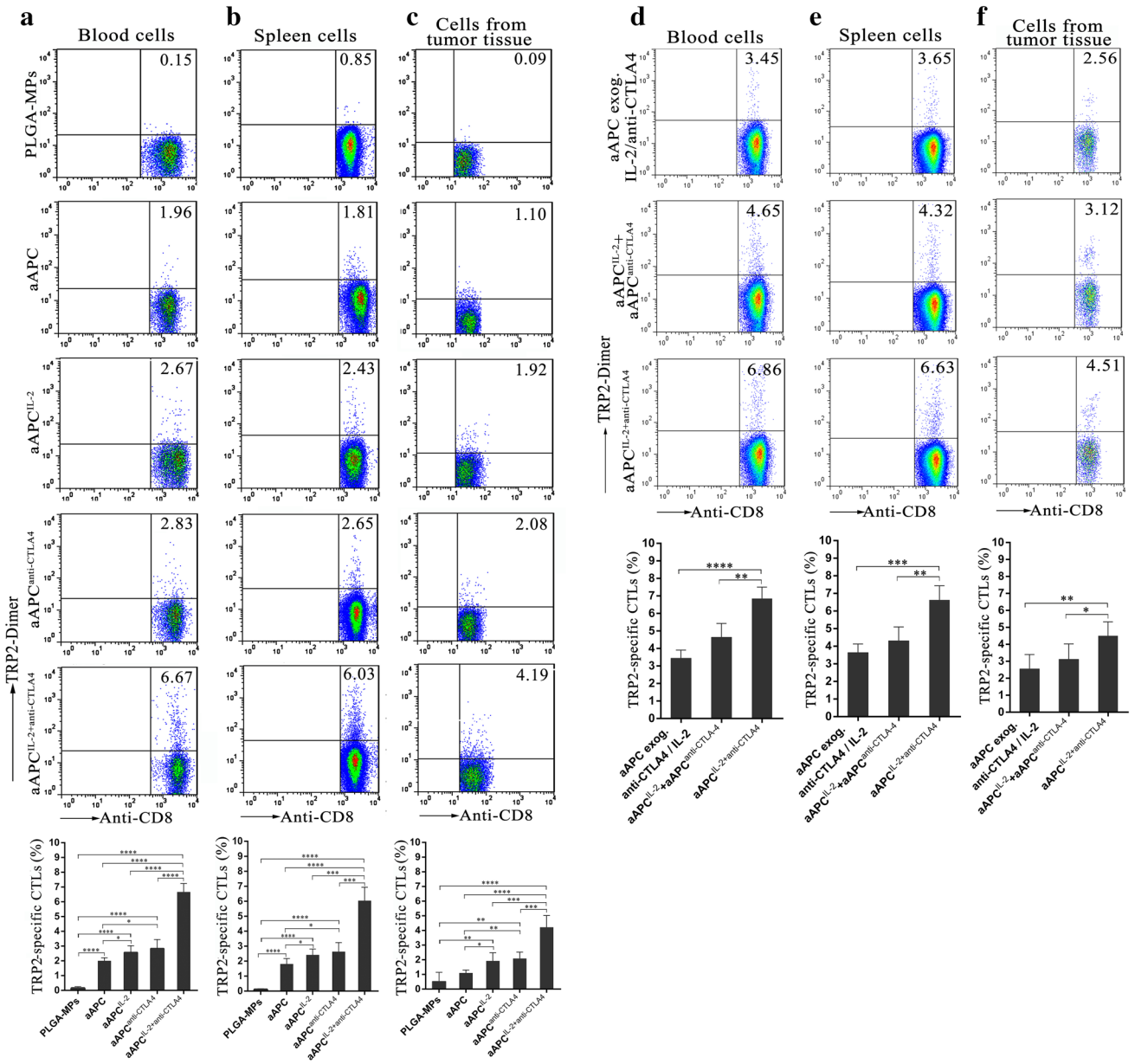

Fig. 6 Paracrine co-release of IL-2 and anti-CTLA-4 from aAPC augmented melanoma antigen-specific CTL responses in a mouse melanoma model. At the endpoint (day 28), the frequencies of $TRP2_{180–188}$-specific CTLs were detected in peripheral blood, spleens and tumor tissues from each treatment group. **a–c** Percentages of $TRP2_{180–188}$-specific CTLs in the $CD8^+$ T cell populations in the treatment groups of blank PLGA-MPs, aAPC, $aAPC^{IL\text{-}2}$, $aAPC^{anti\text{-}CTLA4}$, and $aAPC^{IL\text{-}2+anti\text{-}CTLA4}$. **d**, **f** Percentages of $TRP2_{180–188}$-specific CTLs in the $CD8^+$ T cell populations in the treatment groups of aAPC plus exogenous IL-2/anti-CTLA-4, $aAPC^{IL\text{-}2}$ + $aAPC^{anti\text{-}CTLA4}$, and $aAPC^{IL\text{-}2+anti\text{-}CTLA4}$; $n = 7$ mice in each group. *The numbers in top right of dot plots* represented the percentage of $TRP2_{180–188}$ dimer-positive cells in the $CD8^+$ T cell population. A two-tailed, unpaired Student's *t* test (GraphPad Prism 6.0) and ANOVA with post-test and multiple comparison correction (SPSS18.0, IBM) were used to analyze the differences between groups

Discussion

Numerous studies have reported the promising capability of bead-based aAPCs to expand tumor-specific T cells ex vivo for adoptive immunotherapy [10, 16]. However, conventional aAPCs have mainly been formulated on an un-biodegradable scaffold that has hindered their use in vivo for active immunotherapy. Recently, PLGA-MNPs, an FDA-approved polymer whose safe use in humans has been documented over the past 30 years [21, 28], have been used to prepare bead-based aAPCs by co-coating the pMHC complex and anti-CD28 onto MNPs

and allowing for paracrine release of IL-2 for ex vivo expansion of antigen-specific $CD8^+$ and $CD4^+$ T cells [29–31]. Furthermore, ellipsoidal PLGA-MNPs have been co-coupled with the pMHC complex and anti-CD28 to expand pMEL transgenic $CD8^+$ T cells in vitro and in a mouse model pre-transfused with pMEL $CD8^+$ T cells [32, 33].

Unlike previous studies, the present report not only illustrates the in vivo effects of biodegradable aAPCs fabricated using PLGA-MPs in a native T cell repertoire, but also is the first study to report aAPCs presenting an additional activating signal (IL-2) and an anti-inhibitory signal (anti-CTLA-4) in a sustained paracrine manner. These aAPCs showed a markedly enhanced capability to activate and expand antigen-specific T cells in vitro and inhibit tumor growth in vivo, as compared with conventional two-signal aAPCs. Moreover, the co-release of IL-2 and anti-CTLA-4 not only elicited 2- or 3-fold greater effects compared with those resulting from the single release of IL-2 or anti-CTLA-4 from $aAPC^{IL\text{-}2}$ or $aAPC^{anti\text{-}CTLA4}$, but also achieved the desired synergistic effects in vivo, as compared with combined injections of $aAPC^{IL\text{-}2}$ and $aAPC^{anti\text{-}CTLA4}$ or aAPC injections alongside systemic use of IL-2/anti-CTLA-4. These data emphasize the feasibility and importance of the combined use and paracrine co-delivery of more costimulatory molecules and cytokines in future clinical approaches. As is well documented, IL-2 stimulation and CTLA-4 blockage can elicit vigorous T cell responses by modulating two opposing cell signaling networks [34, 35]. Here, we found that anti-CTLA-4 mAbs released from aAPCs may block the inhibitory signaling pathway between activated TRP2-specific CTLs and tumor cells or natural APCs in vivo or in vitro. More importantly, antigen-targeted and sustained paracrine delivery can result in accumulation of a high level of cytokines and antibodies in the synaptic contact region between antigen-specific T cells and aAPCs or natural APCs at a much lower dosage than used in systemic administration, which usually leads to toxicity and adverse effects [36].

In this study, $aAPC^{IL\text{-}2}$ and $aAPC^{anti\text{-}CTLA4}$ were found to have an encapsulation efficacy and release profile similar to those of $aAPC^{IL\text{-}2+anti\text{-}CTLA4}$, thus indicating that a cytokine with a low molecular weight and an antibody with a high molecular weight did not impair each other in the encapsulation or release process. The encapsulation and release efficacy of each protein depend primarily on the protein dose and size of the molecule. Therefore, the amount of each protein used for co-encapsulation must be titrated according to its function and molecular weight to achieve an appropriate release profile with minimal interference. Here, 2.5 μg of IL-2 and 12.5 mg of anti-CTLA-4 were used with 100 mg of a PLGA polymer, owing to their distinct functions. IL-2 can effectively activate T cells at a concentration as low as pg L^{-1}, whereas anti-CTLA-4 requires a much higher dose to block the CTLA-4 molecules expressed on activated T cells. An encapsulation efficacy of 80% for both IL-2 and anti-CTLA-4 was achieved, and cumulative release efficacies of 81% for IL-2 and 92% for anti-CTLA-4 were observed, which were sufficient for T cell expansion resulting from the targeted and sustained release features of encapsulation. The amount of H-K^b/TRP2-Ig and anti-CD28 coupled onto aAPC beads also must be optimized. Our previous studies have indicated that aAPCs coupled to H-$2K^b$/peptide-Ig ranging from 10 to 20 μg/10^8 aAPCs display a comparable ability to target and expand antigen-specific CTLs, whereas a dose of less than 10 μg does not lead to a clinical efficacy as good as the present regimen. Therefore, 10 μg of H-$2K^b$/TRP2-Ig was used herein to achieve a theoretical density of 3000 H-$2K^b$-Ig molecules per μm^2. However, we cannot exclude the possibility that a dose greater than 20 μg might result in better effects. The ratio of H-$2K^b$/TRP2-Ig:anti-CD28 was also optimized with the best effects at 1:1.

It is also notable that the aAPCs displayed only one predominant epitope of the TRP2 antigen in the format of H-$2K^b$/$TRP2_{180–188}$ dimers. To elicit more powerful T cell responses, multiple epitopes derived from tumor antigens should be used in future approaches. Therefore, one of the limitations of the bead-based aAPC strategy is the requirement of well-defined tumor antigens and their predominant T cell epitopes. For tumors without well-characterized antigens, the aAPC platform may focus on the sustained co-delivery of multiple second-/third-signaling molecules and multivalent immunogens from tumor membrane antigens or cell lysates.

In summary, a polyfunctional polymeric aAPCs system, termed $aAPC^{IL\text{-}2+anti\text{-}CTLA4}$, was developed, in which biodegradable biomaterial (PLGA-MPs) was used as a scaffold, and an additional activating signal (IL-2) and anti-inhibitory signal (anti-CTLA-4) were presented by paracrine delivery. Cytokines and antibodies can be efficiently co-encapsulated in PLGA-MP-based aAPCs and co-released without obvious interference from each other. The targeted, sustained co-paracrine release of IL-2 and anti-CTLA-4 achieved enhanced and synergistic effects in expanding tumor antigen-specific CTLs and inhibiting tumor growth. The precise mechanisms of T cell responses and optimization of both the aAPC system and therapeutic regimen remain to be further investigated. This study provides a foundation for future approaches using bead-based aAPCs for the treatment of tumors and infectious disease.

Acknowledgements This work was supported by the National Natural Science Foundation of China (81172823, 81372448) and

the Science and Technology Support Program of Jiangsu Province (BE2012739).

Compliance with ethical standards

Conflict of interest The authors declare no conflicts of interest.

References

1. Lee SJ, Yang A, Wu TC, Hung CF (2016) Immunotherapy for human papillomavirus-associated disease and cervical cancer: review of clinical and translational research. J Gynecol Oncol 27(5):e51. doi:10.3802/jgo.2016.27.e51
2. Snell LM, Osokine I, Yamada DH, De la Fuente JR, Elsaesser HJ, Brooks DG (2016) Overcoming CD4 Th1 cell fate restrictions to sustain antiviral CD8 T cells and control persistent virus infection. Cell Rep 16(12):3286–3296. doi:10.1016/j.celrep.2016.08.065
3. Hu Z, Xia J, Fan W, Wargo J, Yang YG (2016) Human melanoma immunotherapy using tumor antigen-specific T cells generated in humanized mice. Oncotarget 7(6):6448–6459. doi:10.18632/oncotarget.7044
4. Osada T, Nagaoka K, Takahara M, Yang XY, Liu CX, Guo H, Roy Choudhury K, Hobeika A, Hartman Z, Morse MA, Lyerly HK (2015) Precision cancer immunotherapy: optimizing dendritic cell-based strategies to induce tumor antigen-specific T-cell responses against individual patient tumors. J Immunother 38(4):155–164. doi:10.1097/CJI.0000000000000075
5. Zhang N, Bevan MJ (2011) CD8(+) T cells: foot soldiers of the immune system. Immunity 35(2):161–168. doi:10.1016/j.immuni.2011.07.010
6. Bhargava A, Mishra D, Banerjee S, Mishra PK (2012) Dendritic cell engineering for tumor immunotherapy: from biology to clinical translation. Immunotherapy 4(7):703–718. doi:10.2217/Imt.12.40
7. Bol KF, Schreibelt G, Gerritsen WR, de Vries IJ, Figdor CG (2016) Dendritic cell-based immunotherapy: state of the art and beyond. Clin Cancer Res 22(8):1897–1906. doi:10.1158/1078-0432.CCR-15-1399
8. Kim JV, Latouche JB, Riviere I, Sadelain M (2004) The ABCs of artificial antigen presentation. Nat Biotechnol 22(4):403–410. doi:10.1038/nbt955
9. Butler MO, Hirano N (2014) Human cell-based artificial antigen-presenting cells for cancer immunotherapy. Immunol Rev 257(1):191–209. doi:10.1111/imr.12129
10. Eggermont LJ, Paulis LE, Tel J, Figdor CG (2014) Towards efficient cancer immunotherapy: advances in developing artificial antigen-presenting cells. Trends Biotechnol 32(9):456–465. doi:10.1016/j.tibtech.2014.06.007
11. Goto T, Nishida T, Takagi E, Miyao K, Koyama D, Sakemura R, Hanajiri R, Watanabe K, Imahashi N, Terakura S, Murata M, Kiyoi H (2016) Programmed death-ligand 1 on antigen-presenting cells facilitates the induction of antigen-specific cytotoxic T lymphocytes: application to adoptive T-cell immunotherapy. J Immunother 39(8):306–315. doi:10.1097/CJI.0000000000000136
12. Sun L, Guo H, Jiang R, Lu L, Liu T, Zhang Z, He X (2016) Artificial antigen-presenting cells expressing AFP(158-166) peptide and interleukin-15 activate AFP-specific cytotoxic T lymphocytes. Oncotarget 7(14):17579–17590. doi:10.18632/oncotarget.8198
13. Garnier A, Hamieh M, Drouet A, Leprince J, Vivien D, Frebourg T, Le Mauff B, Latouche JB, Toutirais O (2016) Artificial antigen-presenting cells expressing HLA class II molecules as an effective tool for amplifying human specific memory CD4(+) T cells. Immunol Cell Biol 94(7):662–672. doi:10.1038/icb.2016.25
14. Perica K, Kosmides AK, Schneck JP (2014) Linking form to function: biophysical aspects of artificial antigen presenting cell design. Biochim Biophys Acta 1853(4):781–790. doi:10.1016/j.bbamcr.2014.09.001
15. Bruns H, Bessell C, Varela JC, Haupt C, Fang J, Pasemann S, Mackensen A, Oelke M, Schneck JP, Schutz C (2015) CD47 enhances in vivo functionality of artificial antigen-presenting cells. Clin Cancer Res 21(9):2075–2083. doi:10.1158/1078-0432.CCR-14-2696
16. Perica K, Bieler JG, Schutz C, Varela JC, Douglass J, Skora A, Chiu YL, Oelke M, Kinzler K, Zhou S, Vogelstein B, Schneck JP (2015) Enrichment and expansion with nanoscale artificial antigen presenting cells for adoptive immunotherapy. ACS Nano 9(7):6861–6871. doi:10.1021/acsnano.5b02829
17. Durai M, Krueger C, Ye Z, Cheng L, Mackensen A, Oelke M, Schneck JP (2009) In vivo functional efficacy of tumor-specific T cells expanded using HLA-Ig based artificial antigen presenting cells (aAPC). Cancer Immunol Immunother 58(2):209–220. doi:10.1007/s00262-008-0542-1
18. Lu XL, Jiang XB, Liu RE, Zhang SM, Liang ZH (2009) In vivo anti-melanoma efficacy of allo-restricted CTLs specific for melanoma expanded by artificial antigen-presenting cells. Cancer Immunol Immunother 58(4):629–638. doi:10.1007/s00262-008-0573-7
19. Chiu YL, Schneck JP, Oelke M (2011) HLA-Ig based artificial antigen presenting cells for efficient ex vivo expansion of human CTL. J Vis Exp. doi:10.3791/2801
20. Shen C, Cheng K, Miao S, Wang W, He Y, Meng F, Zhang J (2013) Latex bead-based artificial antigen-presenting cells induce tumor-specific CTL responses in the native T-cell repertoires and inhibit tumor growth. Immunol Lett 150(1–2):1–11. doi:10.1016/j.imlet.2013.01.003
21. Han FY, Thurecht KJ, Whittaker AK, Smith MT (2016) Bioerodable PLGA-based microparticles for producing sustained-release drug formulations and strategies for improving drug loading. Front Pharmacol 7:185. doi:10.3389/fphar.2016.00185
22. Pagels RF, Prud'homme RK (2015) Polymeric nanoparticles and microparticles for the delivery of peptides, biologics, and soluble therapeutics. J Control Release 219:519–535. doi:10.1016/j.jconrel.2015.09.001
23. Iqbal M, Zafar N, Fessi H, Elaissari A (2015) Double emulsion solvent evaporation techniques used for drug encapsulation. Int J Pharm 496(2):173–190. doi:10.1016/j.ijpharm.2015.10.057
24. Shah SR, Henslee AM, Spicer PP, Yokota S, Petrichenko S, Allahabadi S, Bennett GN, Wong ME, Kasper FK, Mikos AG (2014) Effects of antibiotic physicochemical properties on their release kinetics from biodegradable polymer microparticles. Pharm Res 31(12):3379–3389. doi:10.1007/s11095-014-1427-y
25. Donat U, Rother J, Schäfer S, Hess M, Härtl B, Kober C, Langbein-Laugwitz J, Stritzker J, Chen NG, Aguilar RJ (2014) Characterization of metastasis formation and virotherapy in the human C33A cervical cancer model. PLoS One 9(6):e98533. doi:10.1371/journal.pone.0098533
26. Geekiyanage H, Galanis E (2016) MiR-31 and miR-128 regulates poliovirus receptor-related 4 mediated measles virus infectivity in tumors. Mol Oncol 10(9):1387–1403. doi:10.1016/j.molonc.2016.07.007
27. Wang W, Fang K, Li MC, Chang D, Shahzad KA, Xu T, Zhang L, Gu N, Shen CL (2016) A biodegradable killer microparticle to selectively deplete antigen-specific T cells in vitro and in vivo. Oncotarget 7(11):12176–12190. doi:10.18632/oncotarget.7519

28. He C, Ma H, Cheng Y, Li D, Gong Y, Liu J, Tian H, Chen X (2015) PLK1shRNA and doxorubicin co-loaded thermosensitive PLGA-PEG-PLGA hydrogels for localized and combined treatment of human osteosarcoma. J Control Release 213:e18. doi:10.1016/j.jconrel.2015.05.026
29. Steenblock ER, Fadel T, Labowsky M, Pober JS, Fahmy TM (2011) An artificial antigen-presenting cell with paracrine delivery of IL-2 impacts the magnitude and direction of the T cell response. J Biol Chem 286(40):34883–34892. doi:10.1074/jbc.M111.276329
30. Han H, Peng JR, Chen PC, Gong L, Qiao SS, Wang WZ, Cui ZQ, Yu X, Wei YH, Leng XS (2011) A novel system of artificial antigen-presenting cells efficiently stimulates Flu peptide-specific cytotoxic T cells in vitro. Biochem Biophys Res Commun 411(3):530–535. doi:10.1016/j.bbrc.2011.06.164
31. Steenblock ER, Fahmy TM (2008) A comprehensive platform for ex vivo T-cell expansion based on biodegradable polymeric artificial antigen-presenting cells. Mol Ther 16(4):765–772. doi:10.1038/mt.2008.11
32. Sunshine JC, Perica K, Schneck JP, Green JJ (2014) Particle shape dependence of CD8 + T cell activation by artificial antigen presenting cells. Biomaterials 35(1):269–277. doi:10.1016/j.biomaterials.2013.09.050
33. Meyer RA, Sunshine JC, Perica K, Kosmides AK, Aje K, Schneck JP, Green JJ (2015) Biodegradable nanoellipsoidal artificial antigen presenting cells for antigen specific T-cell activation. Small 11(13):1519–1525. doi:10.1002/smll.201402369
34. Jiang T, Zhou C, Ren S (2016) Role of IL-2 in cancer immunotherapy. Oncoimmunology 5(6):e1163462. doi:10.1080/2162402X.2016.1163462
35. Baumeister SH, Freeman GJ, Dranoff G, Sharpe AH (2016) Coinhibitory pathways in immunotherapy for cancer. Annu Rev Immunol 34:539–573. doi:10.1146/annurev-immunol-032414-112049
36. Khoja L, Atenafu EG, Ye Q, Gedye C, Chappell M, Hogg D, Butler MO, Joshua AM (2016) Real-world efficacy, toxicity and clinical management of ipilimumab treatment in metastatic melanoma. Oncol Lett 11(2):1581–1585. doi:10.3892/ol.2015.4069